A Prediction of Laser Spot-to-Cutting Tool Distance in Laser Assisted Micro Milling

ICOMM
2014
No. 32

E. A. Rahim[1], Z. Mohid[1], N. M. Warap[1], M. R. Ibrahim[1], M.I.S Ismail[2]

[1] *Advanced Machining Research Group, Faculty of Mechanical and Manufacturing Engineering, University Tun Hussein Onn Malaysia, 86400 Parit Raja, Batu Pahat, Johor, Malaysia*
[2]*Department of Mechanical and Manufacturing Engineering, Faculty of Engineering, University Putra Malaysia, 43400 Serdang, Selangor, Malaysia*

Abstract

Laser assisted micro milling (LAMM) is one of the methods that used to enhance the ability to manufacture the micro scale product. Laser is used to preheat the workpiece materials prior the machining process. Therefore, reducing the workpiece strength caused by the laser heating need to be controlled to avoid the melting and changing of materials properties. Determining the processing parameters and their effects to the processing characteristics, temperature measurement and the laser spot-to-cutting tool distance are crucially important. In this study, the finite element analysis using ANSYS software was used to predict the heat distribution to characterize the melting and heat affected zone formation. From the results, the estimations of laser spot-to-cutting tool distance together with the allowable depth of cut were determined and applied in the actual LAMM experiment. Meanwhile, the analyses of cutting force and tool wear as an evidence conjunction to the laser heating is applicable to reduce the materials strength was performed.

Keywords: Laser Assisted Micro Milling, Finite Element Analysis, Nd:YAG Laser.

1. Introduction

Machinability to cut the hard material is one of the restraints in the industries, especially on micro scale production. Various types of method were introduced to counter the issue such as using various types of coolant technique, combination of two machining process and fabricate the new coating materials. However, the concentration the research is focusing to improve the product quality and machining characteristics.

The new approach introduced is to enhance and improve the machinability by considering the tool wear, tool life and surface integrity. Hybrid machining process is a combination between two machining method that capable to address the issue. Laser assisted micro milling (LAMM) is one of the methods that widely reported by many researchers. Ding et al. [1] was developing a 3D model to predict the machining characteristic on the laser assisted micro milling of Ti6Al4V, Inconel 718 and stainless steel 422.

Many researchers have reported that the integration of the laser beam for heating and milling process subsequently reduce the cutting forces, material strength and extend the tool life effectively. Kumar and Melkote [2] reported that the effectiveness of the laser-assisted micro milling process can reduce 69% of resultant force with targeted temperature 450-500°C compare to conventional process. Furthermore, Melkote et al. [3] observed that the laser assisted able to extend the tool life, improve the surface quality and machining accuracy.

However, fluctuated temperature distribution on the pulsed laser must be clarified to identify the appropriate distance between tool and laser point. Navas el al. [4] using Nd:YAG laser with 1mm beam diameter and the optimum distance of 45 mm between laser spot and cutting tool in turning process has achieved the maximum reduction of cutting force and minimum tool degradation by applied overheating. Dumitrescu et al. [5] revealed that the appropriate distance for AISID2 material is 85 mm in the laser-assisted turning process. On the other hands, the laser deflection direct to the cutting tool during irradiation must be avoided to prolong the tool life.

Thus, it is important to determine the laser spot-to-cutting tool distance with minimum effect on tool wear. Besides that, laser irradiation plays a significant role on determining the cutting tool location. Therefore, it is essential to predict an accurate temperature changes at appropriate distance in the laser-assisted micro milling process. In this study, computational simulation is performed to predict the temperature distribution in the workpiece and laser spot-to-cutting tool distance. The result from the simulation will be applied in the machining process to confirm that the external heat significantly reduce the materials strength, and concurrently maintaining the surface integrity.

1.1 *Numerical analysis*

The study of the numerical analysis on the temperature distribution by the laser beam was widely reported. Many coordinate systems were applied to express the heat moving such as Cartesian, cylindrical, spherical and ellipsoidal. While various types of function such as Gaussian, Fourier's series and Legendre polynomials to represent the heat flux distribution of the laser heating process. However, the basic model was developed using Fourier's function and applied to the moving heat source [6]. Goldaket et al. [7] modified the model by using double ellipsoidal shape to express the heat flux distribution.

The simplified of Gaussian for heat flux distribution were studied and reported [7, 8]. For deep

penetration welding, the keyhole mechanism brings the significant effect in determining the laser absorption rate. For shallow heating, the keyhole effect can be neglected. The heat flux distribution can be expressed by:

$$q(x,y) = \frac{AKP}{S}\exp\left[\frac{x^2+y^2}{b^2}\right] \quad (1)$$

A is absorption rate (%), *K* is intensity distribution constant. S is irradiated surface area (mm^2) and *b* is the laser beam radius (mm). Mohid et al. [9] reveal that the *K* value of AISID2 materials is 2.5. Meanwhile, the value of *A* might be changed due to material surface conditions. From previous studies, the value of *A* for AISID2 hardened steel workpiece is 0.8 [10]. However, the *K* and *A* asset value will change depended on the laser inclination and could be differed due to the characteristics of the laser delivery system.

2. Model Development and Validation

2.1. Finite Element Analysis

In this study, two laser irradiation angles were considered namely vertical 90° and inclined 55°. The horizontal laser is developed to validate the model while laser inclined 55° is to simulate the actual simulation. A finite element analysis (FEA) model with the width, length and thickness of 8 mm, 10.8 mm and 1 mm respectively was developed. It was prepared in half of the total width to reduce the total number of element and computational processing time. Fig. 1 shows the half model generated using ANSYS software. The total number of element is 60543. To obtain an accurate result, element size in the centre of the model (L1) (scanning path) must be fine compare to conduction area (L2 to L7). Triangle element shape is used due to the conduction process. Table 1 show the values of temperature thermal dependent used in the FEA.

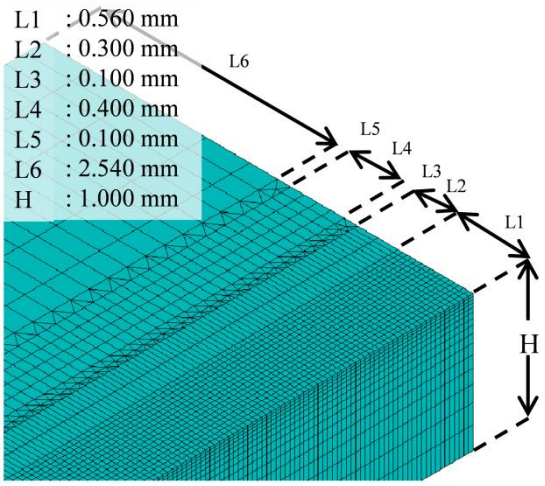

Fig. 1: Mesh and element distribution for FEM model

A three-dimensional finite element model was performed using ANSYS Parametric Design Language (APDL). APDL allows the user to compute the data using transient heat solution, which provides a convenient means of numerical modeling, especially in laser welding processes. In this case, the thermal history of a welded bead as shown in Table 1 is required to indicate the accurate thermal distribution during the process. It requires integration between heat conduction with the respect of time. The program is automatically time stepping with consider the different between two point and it also depending on the pulsed length was applied.

In the simulation, the heat flux was obtained from equation 1 with the impression that the heat was generated by laser on the workpiece surface only. Therefore, the heat flux on the internal can be neglected. For the calculation of the moving heat flux, the position and magnitude of the heat flux are confirmed every time. The distribution of heat flux is depending on the pulsed length time. When the heat flux moved to the next step with different element, the latter distributed heat flux step is deleted. The moving laser beam heat source with depending on pulsed length is applied in order to simulate laser pulsed scanning as shown in Fig. 2. When $t=t_o$, the laser beam was moving in the element between x_1 and x_2 while when $t=t_o+t_p$, it moving from x_1+1 *to* x_2+1 element. The time t_p (ms) at every element can be expressed as equation (2).

$$t_p = \frac{x}{V_S} = 1\ Step \quad (2)$$

Where *x* is the element size in the x axis direction, and V_S (mm/min) is the scanning speed. Basically, when the element size sufficiently small, the moving of laser beam will have precision and recorded heat distribution is more accurate.

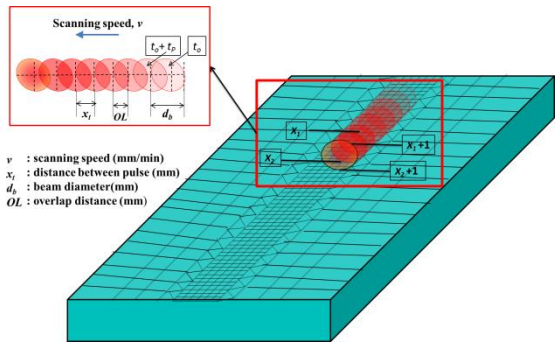

Fig. 2: The step moving heat flux

Table 1
Properties of AISID2 hardened steel [11].

Temperature, T (°C)/ (K)	Thermal Conductivity, *k* x 10^{-6} (W/μm.K)	Specific Heat, *c* (J/Kg.K)	Density, *ρ* X 10^{-15} ($Kg/\mu m^3$)
298 / 571	29.0	412.21	7700
673 / 946	29.5	418.36	7650
1100 / 1373	30.7	421.83	7600
1990 / 2263	32.3	431.00	7560

Several assumptions must be considered to facilitate the simulation work. The assumption consists of (i) the material is homogenous (ii)

simulation is work on transient mode and (iii) the key hole formation can be neglected.

Furthermore, the laser beam shape must be changed to ellipse in order to simulate the inclined laser beam at the angle of 55° .Based from the laser inclination angle, the beam diameter need to be recalculated and used it in the simulation. Fig. 3 shows the method to calculate the laser beam diameter using theorem Pythagoras and the total number of element involved in the entire beam area of vertical and 55° inclined laser orientation.

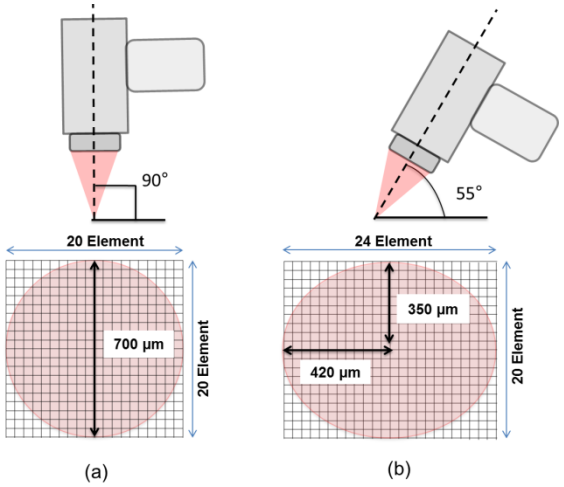

Fig. 3: The total number of element involved in beam area for (a) vertical laser position (90°) (b) inclined laser position (55°)

2.2 Model Validation and Specimen setup

The model can be assumed precise when the depth and width of the melting pool in the numerical simulation are comparable with actual experiment. In this case, the error of less than 10% in melting and HAZ geometry compared to substantial geometry is acceptable to validate the model. The recorded melting temperature in the simulation was ranging from 1713 K to 1850K. It represents the borderline of melting point. The HAZ border lines were defined by deformation temperature of 1268 K.

The actual specimens that exposed to the laser irradiation were cut perpendicular to the scanning direction at the distance of 15 to 20 mm from the starting point. The location is basically based on the stability of heat generated and heat absorption into materials during irradiation process. After that, the specimen has undergone hot mounting process and subsequently through grinding and polishing. Finally, the specimen must be soaked into Nital (ethanol 98% and nitric acid 2%) for 2 minutes. Optical microscope is used to measure the melted and heat affected zone.

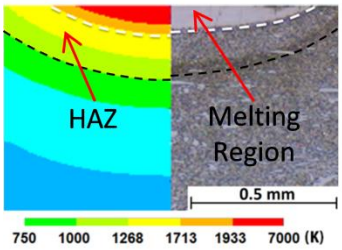

Fig. 4: Comparison of melted zone and HAZ size (P=13.6 W, A=0.8 and K=2.5)

In this study, vertical laser was used to validate the model. An average power (P_{avg}) of 10 W, laser absorption rate of A 80% and K value of 2.5 were applied into the FEA model in order to validate and compare between actual and simulation. The simulation can be accepted if the percentage error on the melting width and depth is less than 10% as shown in Fig. 4. After the model validation was proven, some modification on the laser beam shape must be done to simulate the inclined laser 55^{o} (Fig. 2 (b)).

2.3. Laser Assisted Micro Milling

A diagram of the experimental-set up is presented in Fig. 5. A dynamometer Kistler type 9317B with charge amplifiers was used along with computer to measure and record cutting forces during the machining process. A set of the amplifier complete plug in with DAQ-Charge B was used to collect the signal and convert the signal into the data format.

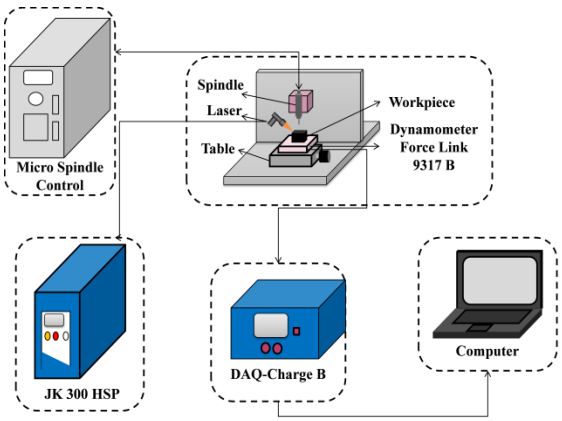

Fig. 5: Laser Assisted micro milling setup

The air bearing spindle with the maximum rotational per minute of 60,000 was installed into the micro milling machine. All the laser assisted micro milling tests were carried out on a hardened AISID2 tool steel plate (59 HRC) with 25 mm length, 50 mm width and 8 mm thickness. A commercially available TiAlN coated carbide ball end mills (two flutes) from Mitsubishi Materials (MS2SB) with a diameter of 300 µm were used in cutting tests. The workpiece surface was preheated using a Nd:YAG pulsed laser with 1064 nm.

Table 2 gives the parameters used for slot milling process. Fig. 6 shows the closed-up view of the

LAMM setup. The laser head was inclined to 55° to avoid the deflection of laser irradiation on the cutting tool. The irradiated heat into the cutting tool will alter its properties.

Table 2
Machining parameters.

Parameters	Machining Parameters
Laser Power, P_{avg} (W)	8, 10
Laser spot-to-tool Distances, $X_{t\text{-}b}$ (µm)	600, 800, 1000
Scanning Speed V_s (mm/min)	210
Spindle Speed, (RPM)	35,000
Feed rate, f_r (mm/min)	210
Depth of Cut,t_c(µm)	20, 40, 60

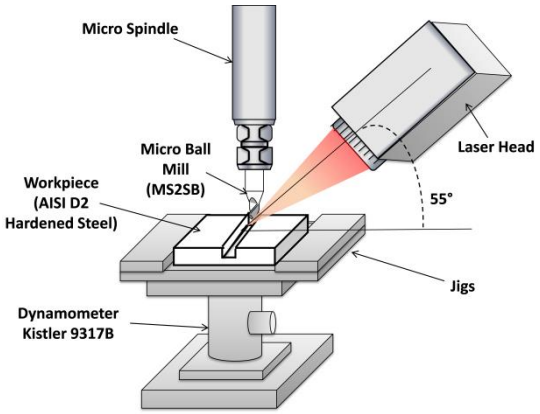

Fig. 6: Closed-up view of LAMM setup

2.4 Determination of laser spot-to-cutting tool distance

The laser spot-to-cutting tool distance is essential in LAMM process. The pre-heating process gives an opportunity to soften the workpiece surface. Fig. 7 shows the schematic diagram of LAMM theory. T_{bc} is the temperature produced by laser beam, meanwhile T_c is a cutting temperature generated by the machining process. As the laser irradiation time increases, the temperature of workpice surface increase until maximum value. The maximum value is depends on the laser parameters. However, the maximum value is not suitable for cutting process due to the materials properties changes. Therefore, it is vital to determine the approximate laser spot-to-cutting tool distance based on the cooling rate of AISI D2 hardened steel. In addition, the irradiated temperature must be in range of workpiece deformation temperature prior the cutting process is taking place.

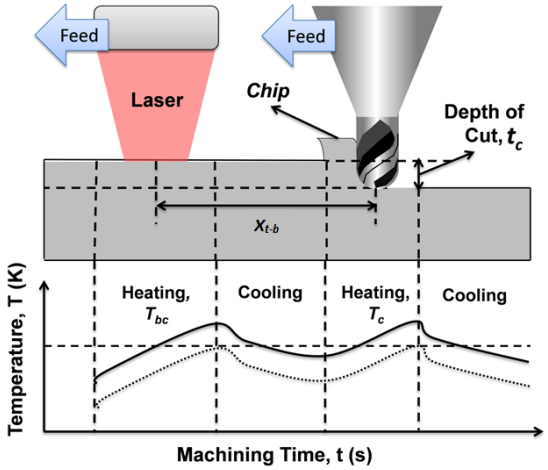

Fig. 7: The determination of laser beam-to-cutting tool distance and the depth of cut.

Laser spot-to-cutting tool distance is determined by referring to the temperature generated at the centre irradiation line in FEA. Pre-heating process using pulsed wave laser creates massive fluctuation of temperature value. Fig. 8 shows the numerical result of temperature and the cross-sectioned view of the workpiece at the distance of 1 mm from the starting point. Cooling time between pulsed (Fig. 2) was sufficient for specimen to chill down approximately from 2000 to 300 K. Therefore, equation 3 can be used to determine the laser spot-to-cutting tool distance (µm).

$$Laser - to - tool\ Diastance, x_{t-b} = T_d(V_s) \qquad (3)$$

Cooling period from peak temperature to deformation temperature of AISI D2 was recorded as a time different, T_d (min). Total cooling time taken must be multiplied by the scanning speed, V_s to obtain the laser spot-to-cutting tool distance.

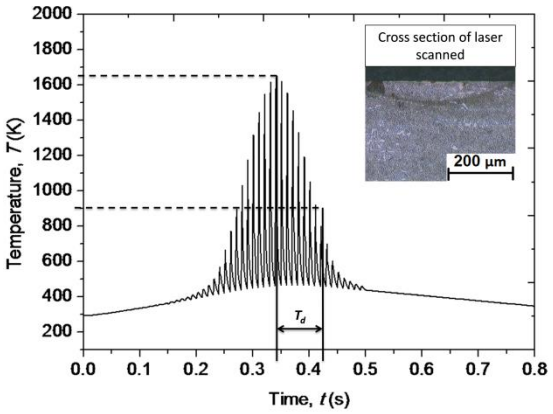

Fig. 8: Temperature changes at the scanning line centre (calculated using A=80%, t_p=2ms *and* P_{avg}=8W)

Based on the calculation, with applied P_{avg}, t_p and A of 8 W, 2 ms and 80% respectively, the laser spot-to-cutting tool distance was determined approximately 300 µm. Meanwhile, the distance increases to 350 µm when the P_{avg} of 10 W was

employed. However, the measured laser beam diameter is 700 µm. Therefore, in order to avoid the the laser beam irradiate into the cutting tool, the minimum distance of 600 µm should be employed. Fig. 8 shows the prominence to define laser spot-to-cutting tool distance and its importance to control the irradiation temperature.

3. Result and Discussion

3.1 Thermal analysis

Fig. 9 (a) and (b) shows the results of experimental and simulation data for melting pool depth and width for constant absorption rate (*A*) of 0.8. It was noted that the error of melting width becomes smaller when the *K* value of 2.5 is applied. However, the error of melting depth increases when the *K* value is 3. This is due to the laser intensity on Gaussian distribution in simulation, which was determined by the total energy density. The greater value of *K* is used produced higher laser beam density and this does not coincide with the actual situation during irradiation.

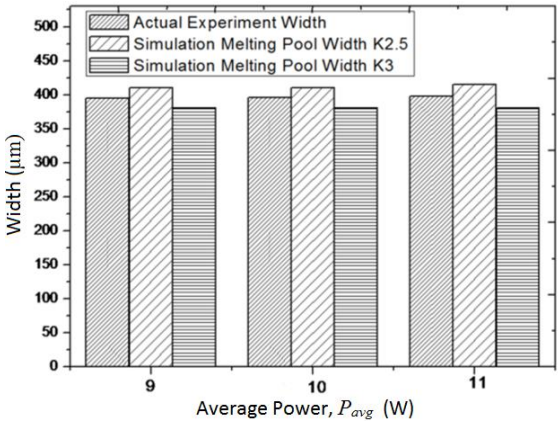

(a)

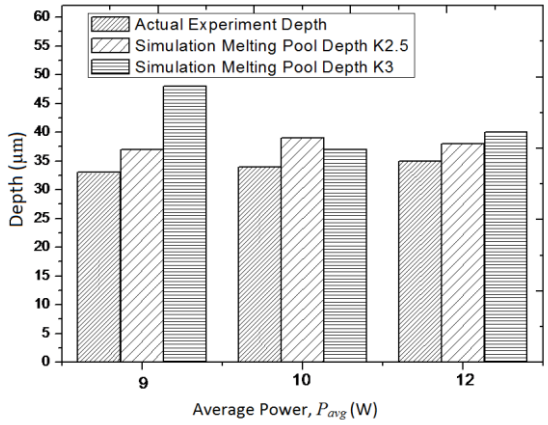

(b)

Fig. 9: Comparison result between experimental and simulation data with different *K* values for (a) Melting pool width (b) Melting pool depth

Furthermore, laser power also plays a significant role to the formation of the melting pool. As the laser power increases from 10 to 12 W, the melting width and depth were not substantial changes as shown in Fig. 4. In the case average power 9 W, the measured melting width and depth were bigger than the actual experiment. The divergence of this result was due to the instability of laser power per unit pulse.

Fig. 10 shows the effect of *K* value in the Gaussian distribution. The *K* value gives the significant effect on the laser intensity. When the *K* value is larger, the intensity is higher but the diameter of the beam was decreased. It can be explained by the heat flux distribution in the simulation, where the Gaussian beam mode is depended on the *K* and *A* values. Ismail et al. [12] was using *K* equal to 3 to simulate the micro welding process with consider the key hole formation but in these cases, the smaller value of *K* need to be used to produce conduction-heating mode compared to the penetration mode in the simulation. This method subsequently generates lower laser beam intensity and the key hole formation can be avoided.

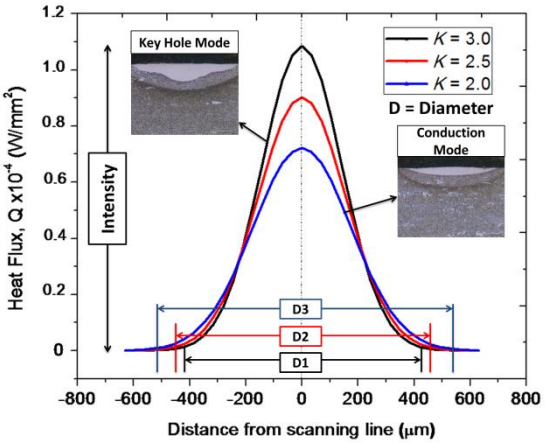

Fig. 10: The effect of *K* value on the diameter and laser beam intensity

3.2 Cutting force

Fig. 11 shows the effect of depth of cut and LAMM process on cutting force. The result shows that the thrust force significantly increases with increasing the depth of cut from 20 to 40 µm. In all cases, the trust force is lower using LAMM with P_{avg} of 8 W and T_p of 2 ms. In addition, there is no molten region occurred under this condition. In contrast, by using the same T_p and different P_{avg} of 10 W, the thrust force was significantly increased. This is due to the temperature of workpiece surface was over the workpiece melting temperature. As a result, a martensitic phase was transformed a few micron underneath the workpiece surface due to the hardening effect. This process is commonly known as the tempering process as shown in Fig. 12 (a). Otherwise, the formation of melted layer or recast layer will be occurred as shown in Fig. 12 (b), where the material property was transformed to the ceramic nature thus, produces higher material hardness. It can be observed that the preheating temperature changes the workpiece microstructure from ferrite into austenite. In the austenitic form, steel can dissolve a lot more carbon to precipitate carbides (Fig. 12 (c)) [13]. In addition, ineffective chip removal also contributes to the higher thrust force.

In the meantime, as the depth of cut increases from 20 to 60 µm the average thrust force was declined. This phenomenon is due to the formation of chipping on the cutting tool edges. In conventional machining process, the chipping was occurred after 5 mm of cutting length. However, in LAMM, chipping was occurred after 10 mm of cutting length. It indicates that surface pre-heating using a laser beam significantly influenced the machining performance especially to prolong the cutting tool life. In this phenomenon, the temperature generated by the laser is on the deformation temperature and the resultant effect softening happen [2]. Therefore, further study need to be conducted to understand the effect of laser parameter on the pre- heating process of AISI D2 materials.

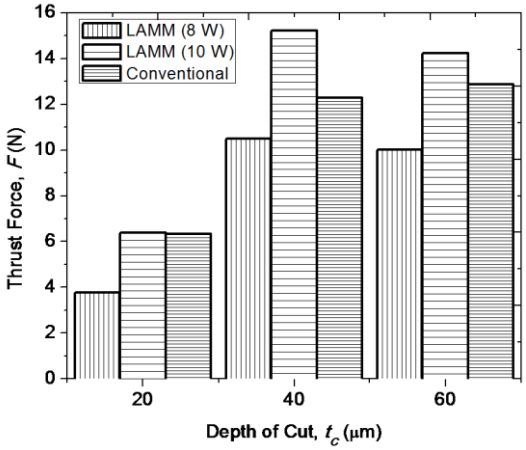

Fig. 11: The effect of machining parameters on cutting force

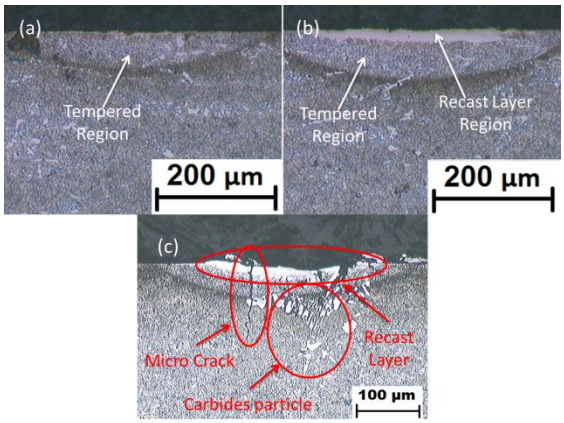

Fig. 12 :Optical micrograph with 200X magnification of cross section of (a) P_{avg} 8 W, T_p 2 ms (b) P_{avg} 10 W, T_p 2 ms (c) LAMM with P_{avg} 10 W, t_c 20 µm, D_x 600 µm.

3.3 The effect of laser spot-to-cutting tool distance

In this study, the effect of the laser spot–to-cutting tool distance was observed and compared with conventional micro milling process. The cutting force was measured at different distance, specifically 600, 800 and 1000 µm.

Fig. 13 shows the average forces of feed, tangential and thrust force in different laser-to-tool distance. The average thrust force at three laser spot–to-cutting tool distances (600, 800 and 1000 µm) rose significantly. However, the average force for feed and tangential force was no longer substantially different. Average thrust force at the distance of 1000 µm is higher compared to the conventional machining due to the tempering effect and commonly known as hardening effect. It is also caused by rapid laser heating up over deformation temperature and subsequently it cooling rapidly. In contrast, the average thrust force at the distance of 600 µm is lower. It indicates that this distance is capable of ensuring that the material is in a delicate situation during cutting process.

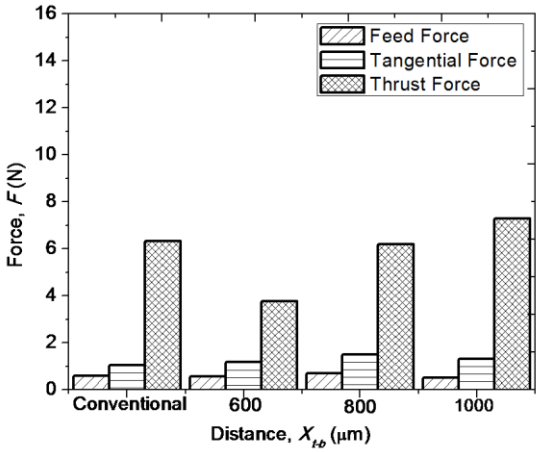

Fig. 13: The average cutting force at different laser spot–to-cutting tool distance and its comparison with conventional machining.

3.4 Tool wear

In this work, the flank faces of worn tools were examined using a digital microscopic analyzer. Fig. 14 shows the variation of wear patterns at all tested conditions. The image shows an evidence of chipping occurred on the flank face. The effect of laser parameter and depth of cut give the prominent effect on the tool wear. The chipping area was critically increases when the depth of cut, t_c increase from 20 to 40 µm. However, rapid progressive of flank wear and chipping were observed at the depth of cut to 60 µm. This rapid progress contributes to the premature tool failure and brakeage. This phenomenon is due to the higher depth of cut produces thicker uncut chip thickness. In terms of ball end mill cutting tool, the effective of cutting process at the bottom surface is poor and is compelling to the rubbing process. Furthermore, the ineffectiveness of chip removal causes chips re-enters into the cutting region.

It can be noted in Fig. 15 that the chipping area of conventional machining was more severe than LAMM at the P_{avg} of 8 W. Furthermore, the chipping region at P_{avg} of 10 W seems to be larger than P_{avg} of 8 W. This can be explained by the formation of carbide particle underneath the workpiece surface (Fig. 12 (c)). The formation of carbide particle contributes to the chipping phenomenon because the hardness at the area is higher compared to the bulk material. In terms of laser spot–to-cutting tool distance, the chipping was no significantly different compare to the conventional process. However, the increment of distance will increase the chipping area due to the tampered effect and microstructure changes.

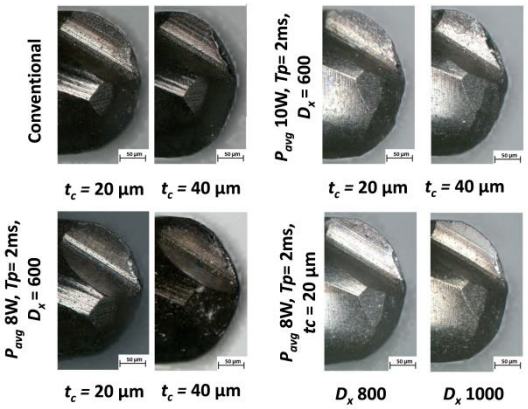

Fig. 14: Optical micrograph image of cutting tool at the magnification of 200X

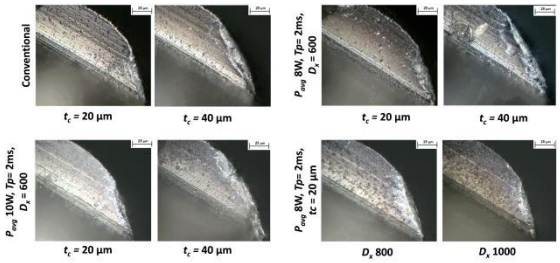

Fig. 15: Optical micrograph image of cutting tool focused at the chipping region with the magnification of 500X.

4. Conclusions

From the simulation and experimental work, it can be concluded that:

i. It can be suggested that the *K* and *A* values for AISI D2 material are 2.5 and 80%. However, it can be modified depends on the actual machining condition.

ii. Inclined laser beam position tends to avoid the irradiation into the cutting tool, but it will reduce the power beam density.

iii. The laser spot–to-cutting tool distance of 600 µm can be applied in LAMM process. The temperature of heat at this location ranging from 800 to 950 °C with minimum microstructure changes.

iv. Pre-heating process using a laser was capable to produce a layer without melting region. This scenario helps to reduce cutting force and changes of material properties can be minimized.

v. Results show that the LAMM process significantly reduces the tool wear and cutting force. However, the optimum laser parameters must be properly selected to avoid the tempering effect during the LAMM process.

Acknowledgements

The author would like to acknowledge financial support from the Ministry of Education of Malaysia under the MyBrain15 program and Science Fund Research Grant (S020) from the Ministry of Science, Technology and Innovation Malaysia (MOSTI). The authors would like to extend their acknowledgement to Mitsubishi Materials for supplying the cutting tools.

References

[1] H. Ding et al., “Thermal and mechanical modeling analysis of laser-assisted micro-milling of difficult-to-machine alloys,” International Journal ofMaterial Processing Technology, 2012; 212: 601-613.

[2] M. Kumar et al., “Process capability study of laser assisted micro milling of a hard-to-machinematerial,” International Journal of Manufacturing Process, 2012; 14: 41-45.

[3] S. Melkote et al., “Laser assisted micro-milling of hard-to-machine materials,” CIRP-Annals Manufacturing Technology., 2009; 58: 45-48.

[4] V. G. Navas et al., “Mechanisms involve in the improvement of Inconel 718 machinability by Laser Assisted Machining (LAM),” International Journal of Tool & Manufacturing Technology, 2013; 46: 1-29.

[5] P. Dumitrescu et al., “High-power diode laser assisted hard turning of AISI D2 tool steel,” International Journal of Tool & Manufacturing Technology, 2006; 46: 2009-2016.

[6] J. Goldak et al., “Computational Welding Mechanics,”Library of Congress Cataloging in Publication Data, Springer Science: 2005, 22.

[7] J. Goldak et al., “High-power diode laser assisted hard turning of AISI D2 tool steel,” International Journal Tool & Manufacturing Technology, 2006; 46: 2009-2016.

[8] M. I. Ismail et al.,“Experimental Investigation on Micro-Welding of Thin Stainless Steel Sheet by Fiber Laser,” American Journal of Engineering and Applied Sciences, 2011; 4: 314-320.

[9] Z. Mohid et al., “Determination of Heat Flux Intensity Distribution and Laser Absorption Rate of AISID2 Tool Steel,” Applied Mechanics & Materials, 2014; 465-466: 730-734.

[10] G. Singet et al., “Finite Element Modeling of Laser-Assisted Machining of AISI D2 Tool Steel,” InternationalJournalMaterials&ManufacturingProcessing, 2013; 28: 443-448.

[11] M. Pradhan, Experimental Investigation and Modelling of Surface Integrity, Accuracy and Productivity Aspects In EDM of AISI D2 Steel, National Institute of Technology- PHD thesis. Roukela : 2010.

[12] M. I. Ismail et al., Experimental Investigation on Micro-Welding of Thin Stainless Steel Sheet by Fiber Laser. American Journal of Engineering and Applied Sciences. 2011: 4: 314-320.

[13] R. G. Song, K. Zhang & G. N. Chen, Electron beam surface remelting of AISI D2 cold-worked die steel. Surface & Coating Technology 2002: 157: 1-4.